Available online at www.sciencedirect.com
SCIENCE DIRECT®
International Journal of Thermal Sciences 43 (2004) 431–442
International Journal of Thermal Sciences
www.elsevier.com/locate/ijts

Peculiarities of boiling heat transfer on capillary-porous coverings

Mieczyslaw E. Poniewski

The Kielce University of Technology, Al. 1000-lecia P.P. 7, 25 314 Kielce, Poland

Received 30 January 2003; accepted 6 October 2003

Abstract

The paper discussed specific features of boiling heat transfer on developed industrial micro-surfaces and surfaces with capillary porous coverings obtained with various techniques. Boiling on such surfaces is characterised by the occurrence of a few physically disparate hysteresis phenomena, as well as by the different course of *nucleate boiling crisis* as compared with smooth surfaces. Attempts at modelling the *nucleation hysteresis* and that of the *I-kind* and also *nucleate boiling crisis* for various surfaces with capillary-porous covering were presented. Apart from the discussion of other researchers' investigation results, the physical interpretation of *II-kind hysteresis* phenomenon was given. A theoretical model congruent with experimental data for metal fibrous coverings was also provided. The properties of three hydrodynamic models of *nucleate boiling crisis* were discussed as well. The statistical concept of the maximum point process was employed for the sake of *intra-layer boiling crisis* modelling; the result obtained was consistent with the experiment.

Keywords: Boiling on porous covering; Boiling crisis; Hysteresis

1. Introduction

Developed micro-surfaces, manufactured by industries, and capillary porous structures, covered with various techniques, do not only enhance heat transfer but also might cause various hysteresis phenomena and change the course of *nucleate boiling crisis* when compared with smooth surfaces. Many variations of boiling heat transfer hysteresis are much more clearly manifested on surfaces with capillary porous coverings than on smooth surfaces. Experimental boiling hysteresis curves show diversified shapes, which depend on geometrical and thermal parameters of a capillary porous covering and the liquid physical properties. The reason for $\dot{q}_{\max}$ (or $\dot{q}_{c}$) increase on developed micro-surfaces and porous structures is thought to be a smaller diameter of vapour bubbles breaking away and increased frequency of departure, increase in the number of nucleation centres in comparison with smooth surfaces and also hampered bubble coalescence into a vapour film, which might cause obstruction to the liquid flow to the porous covering.

2. Heat transfer hysteresis

2.1. Hysteresis phenomena diversity

The application of porous coverings to heat transfer enhancement requires stable and unambiguous course of boiling curves. Hysteresis is generally regarded as a disadvantageous phenomenon, which prevents thermal stabilisation of the systems emitting high heat flux densities. Due to the analysis of experimental boiling curves, it is possible to differentiate typical hysteresis kinds shown in Fig. 1:

(a) *nucleation hysteresis*, termed also *zero boiling crisis* or *temperature overshoot*;
(b) *I-kind hysteresis*, also *intra-layer* (*internal*) *boiling crisis*, *reverse hysteresis loop*, being characterised by the decrease in heat transfer coefficient after the decrease in heat flux; it occurs after the flux has reached its maximum density;
(c) *II-kind hysteresis, simple hysteresis loop, hysteresis with temperature deviation*, characteristic of which is the heat transfer coefficient increase at the heat flux diminishing, prior to the flux reaching the maximum density;
(d) hysteresis characterised by the heat transfer coefficient decrease at the decrease in the flux, before it reaches the maximum density;

E-mail address: tmpmp@tu.kielce.pl (M.E. Poniewski).

1290-0729/$ – see front matter
doi:10.1016/j.ijthermalsci.2003.10.002

Nomenclature

a	cell density	m^{-2}
A	cross-section, surface	m^2
b	dried cell density	m^{-2}
C_i	constants	
d	micro-fin dimension	m
D	diameter	m
E'''	specific work, potential or kinetic energy	$J{\cdot}m^{-3}$
f	field ratio, function	
g	gravity	$m{\cdot}s^{-2}$
h	heat transfer coefficient	$W{\cdot}m^{-2}{\cdot}K^{-1}$
h_{lg}	heat of evaporation	$J{\cdot}kg^{-1}$
H	height	m
k	constants, thermal conductivity	$W{\cdot}m^{-1}{\cdot}K^{-1}$
K	permeability	m^2
L	path	m
m	mass	kg
	fin parameter	m^{-1}
n	number of layers	
N	nucleation centre density	m^{-2}
O	perimeter	m
p	pressure	Pa
	probability	
$\dot{q}$	heat flux	$W{\cdot}m^{-2}$
R	radius	m
	gas constant	$J{\cdot}K^{-1}{\cdot}kg^{-1}$
T	temperature	K (°C)
u	velocity	$m{\cdot}s^{-1}$
γ	pore diameter distribution function	m^{-1}
δ	layer thickness	m
ε	porosity	
ϑ	slope of a boiling curve p–T	$N{\cdot}m^{-2}{\cdot}K^{-1}$
θ	wetting angle	deg
λ	wavelength	m
	Poisson process intensity	
Π	percolation threshold	
μ and ν	dynamic and kinetic viscosity	$N{\cdot}s{\cdot}m^{-2}$, $m^2{\cdot}s^{-1}$
ν	dry-out intensity	
ρ	density	$kg{\cdot}m^{-3}$
σ	surface tension	$N{\cdot}m^{-1}$

Subscripts

a	active
ad	additional
ap	aperture
c	critical
cc	conduction and convection
del	delay
ef	effective
ej	ejection
f	fin or friction
g	gas or vapour
gr	grain
h	hydrodynamic
hst	hysteresis
ib	initiation of boiling
KH	Kelvin–Helmholtz
l	liquid
lg	liquid–gas/vapour
m	modulated
max	maximum
min	minimum
n	nominal
p	pore
pf	perforation
pl	plane
s	solid
sat	saturation
sb	surface boiling
sk	skeleton
vs	viscous
w	wall-saturated liquid
σ	surface tension
2ph	two-phase

Superscripts

cell	single active cell
$*$	characteristic, specific or modified
$^-$	mean value

(e) hysteresis, a particular characteristic of which is, first, decrease and then increase in heat transfer coefficient while the heat flux is reduced, after the flux has reached its maximum density ("*d*" and "*e*" found rarely);
(f) *boiling crisis hysteresis*, characterised by the increase in the maximum heat flux while the flux increases again [10,12].

2.2. Nucleation hysteresis

Three various hypotheses explaining *nucleation hysteresis* are put forward, namely: the total filling of inactive pores with the liquid and the resistance of medium flow through the capillary-porous layer [16], the dynamic change in the wetting angle in the function of the liquid motion direction [3] and various geometry of pores occupied by vapour for boiling incipience and fading [9]. Theoretical considerations referred mainly to the results of experimental investigations where porous coverings made of sintered powders were used.

For the sake of calculations of the surface superheating, H. Zhang and Y. Zhang [16] relied on the following dependencies required for a balance of vapour nucleus created inside a pore: the condition of pressure balance for

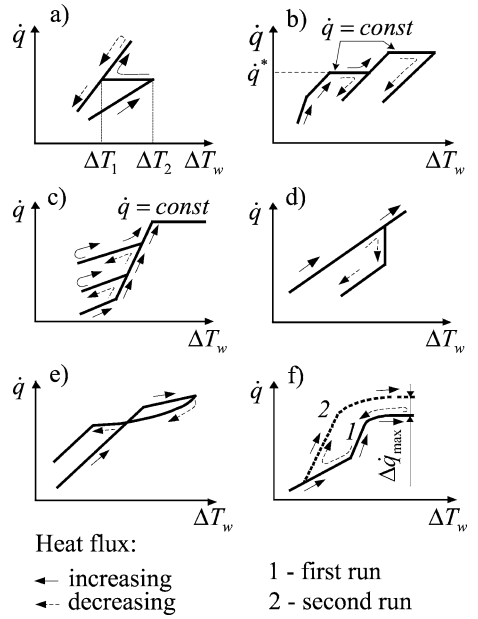

Fig. 1. Kinds of boiling heat transfer hysteresis on capillary-porous coverings [10,12].

the liquid, vapour and inertial gas contained in a pore, the Clausius–Clapeyron ideal gas equation of state for inertial gas, which determines the boiling curve inclination:

$$\Delta T_1 = \Delta T_{w,1} = \Delta T_{w,1} - T_{sat} = T_{sat}\left(2\sigma_{lg}/R - 3m_g R_g T_g/4\pi R^3\right)/h_{lg}\rho_g \quad (1)$$

If residual quantities of vapour or gas do not linger in pores, $m_g = 0$, the superheating is expressed by the dependence:

$$\Delta T_2 = 2\sigma_{lg} T_{sat}/h_{lg}\rho_g R \quad (2)$$

Obviously $\Delta T_2 > \Delta T_1$, this means that the superheating of the surface, indispensable to boiling initiation, is in this case much higher than in the situation when residual quantities of vapour, or gas, are contained in the pore. Thus the temperature rise characteristic of *nucleation hysteresis* amounts to

$$\Delta T_{hst} = \Delta T_2 - \Delta T_1 = 3m_g R_g T_{sat} T_g/4\pi R^3 \rho_g h_{lg} \quad (3)$$

Prior to the boiling initiation, in sintered powder porous layers, the residual quantities of inertial gas or vapour are unable to leave the inside of the pore, in spite of the significant superheating of the heating surface. It is caused by the following factors: liquid static pressure, high resistance of flow through the porous structure and capillary forces. The increase in superheating leads to the vapour accumulation inside the porous covering. Hence, the superheating $\Delta T_2(2)$ is larger than $\Delta T_1(1)$, sufficient for sustaining the boiling. With appropriate pressure growth, some vapour leaves the porous covering, which leads to pressure drop and explosive boiling of a certain amount of liquid. Explosive boiling enhances heat transfer and the surface superheating decreases reaching a stable value of ΔT_1.

Therefore the temperature rise accompanying *nucleation hysteresis* ΔT_{hst} is properly described with Eq. (3). The rise is related to the pore ability to accumulate gas (or vapour), m_g, the liquid thermal properties $h_{lg}\rho_g$ and the thermodynamic state of the residual quantities of gas (or vapour), T_g, T_{sat} [16].

Ko et al. [3] suggested their own interpretation of temperature rise ΔT_{hst}, partially based on the same assumptions as in the previous model. With some simplifications, sintered powder porous structure was assumed to be composed of vertical capillaries. Other assumptions stated that metal powder grains have the same diameter, all vacant spaces (pores) have the same shape, each vacant space is an active nucleation centre, the porous layer thermal conductance is high, that is, the temperature gradient per layer can be disregarded. The pressure of the liquid column above the heating surface and the porous covering geometrical characteristics were also taken into account. On the basis of these assumptions, the following dependence for *nucleation hysteresis* temperature rise was derived:

$$\Delta T_{hst} = \Delta T_2 - \Delta T_1 = \frac{T_{sat}\Delta\rho_{lg}}{h_{lg}\rho_l\rho_g}\left(Hg\rho_l + \frac{2\sigma_{lg}}{R_{ap}}\cos\theta - p_{sat}\right) - \left(\frac{\Lambda q R_p^2}{k_l} + \frac{2\sigma_{lg}}{\vartheta R_p^2}\right) \quad (4)$$

where Λ is the coefficient characterising the porous covering geometry. Eq. (4) implies that the *nucleation hysteresis* temperature rise will be the larger, the higher is the liquid column above the heating surface $Hg\rho_l$, the lower is the wetting angle value θ, the higher is the surface tension σ_{lg} and the lower is the vaporisation heat, h_{lg}. The porous covering structural parameters Λ also affect the value of ΔT_{hst}. The final conclusions drawn by Ko et al. [3] are that the wetting angle and its dynamic change in the function of the liquid motion direction, that is, the boiling liquid penetration properties have decisive impact on hysteresis.

Neither of the models presented above offers the possibility to predict the temperature rise ΔT_{hst} for preset porous covering structural parameters and the boiling liquid thermal properties.

Malyshenko and Styrikovich [9] believed that the differences in heat flux and the surface superheating for boiling incipience and fading resulted from the different geometry of pores filled with vapour in each of these processes. In porous surfaces, two characteristic radii are found: microhollow opening radius R_{ap} and the minimum radius of a vapour filled pore when the vapour starts getting outside the porous layer R_p. The smaller of the two radii decides about the surface superheating, appropriate for the boiling incipience:

$$\Delta T_{ib} = 2\sigma_{lg} T_{sat}\cos\theta/h_{lg}\rho_g R \quad (5)$$

where $R = \min\{R_{ap}; R_p\}$. As R_{ap} and R_p for porous structures are much larger than R_{ap} for smooth surfaces, the boil-

ing incipience for these structures takes place at smaller ΔT_{ib}. Numerous experimental data confirm this conclusion.

At the same time, the active pores deactivation proceeds far easier because the curvature radius at the pore entrance is the function of the diameters of grains making the porous structure, i.e., it is large enough. Under such conditions thermo-capillary convection can also develop in the micro-layer of the liquid covering the structure skeleton walls. It is caused by the surface inactive and not evaporating liquid impurities. This mechanism can be the cause of *nucleation hysteresis*, far more clearly manifested here than on a smooth surface [9].

The minimum radius of a pore filled with vapour can be calculated when the pore radius distribution function γ and the pore spatial network geometry are known (on the basis of percolation theory [2]). The assumption that the vapour will propagate inside the porous layer along the largest available pores leads to:

$$\int_{R_p}^{R_{max}} \gamma(R)\,\mathrm{d}R = \Pi \tag{6}$$

on the basis of which, it is possible to calculate the pore radius R_p for vapour beginning to leave the layer. Π is percolation threshold [2]. On the basis of Eqs. (5) and (6), the heating surface superheating ΔT_{ib} was calculated for the incipience of water nucleate boiling on capillary-porous coverings made of nichrome sintered powders. The results obtained were congruent with the experiment [9].

2.3. I-kind hysteresis

As far as boiling with *I-kind hysteresis* is concerned, Malyshenko and Styrikovich [9] differentiated two kinds of nucleate boiling, namely I and II kind, for increasing and decreasing heat flux. In the case of the I kind, $\dot{q} < \dot{q}^*$, Fig. 1(b), vapour areas inside the covering do not coalesce and the liquid stays in contact with the heating surface. For a certain characteristic flux, a dissipation change of phase occurs from I to II nucleate boiling kind. It is accompanied by a dramatic increase in relaxation time, when $\dot{q} \to \dot{q}^*$, and *I-kind hysteresis* if $\dot{q}$ values are diminished.

I-kind hysteresis was also termed *hysteresis with memory*, as the shape of the boiling curve when $\dot{q}$ is reduced depends on the remembered value of the surface superheating ΔT_w, at which the heat flux reduction began, Fig. 1(b).

I-kind hysteresis occurs when the porous structure demonstrates high inhomogeneity while pores are being filled with vapour. It takes place in the case of structures of low permeability and low thermal conductivity [9]. Phase transition from I to II nucleate boiling kind corresponds to a certain percolation threshold, when vapour "punctures" the porous covering, i.e., penetrates the pores occupied with the liquid at nucleate boiling initiation. It means that the pores originally occupied with vapour and corresponding to the original percolation threshold Π should be excluded from the spatial network of stochastically distributed pores, which gives

$$\Pi^* = \Pi/(1-\Pi) \tag{7}$$

The minimum radius of pores occupied with vapour under *I-kind hysteresis* conditions is calculated from Eq. (6), where $\Pi = \Pi^*$.

For known R^*, ΔT_1^* is calculated from Eq. (5). Full superheating of the heating surface ΔT_w^* for phase transition I → II nucleate boiling kind is the sum

$$\Delta T_w^* = \Delta T_1^* + \Delta T_2^* \tag{8}$$

where the second term is a mean temperature drop in a vapour layer, δ_g, from the heating surface to the evaporation zone. For known mean grain size D_{gr}, known grain packing geometry and skeletal conductivity k_{sk}, it can be assumed that for densely packed porous structures the values of

$$\Delta T_2^* = \dot{q}^* \delta_g / k_{sk}, \quad \delta_g \approx D_{gr}/4 \tag{9}$$

The values of ΔT_w^*, calculated in accordance with the above stated procedure, are close to the experimental data.

The observations of the *I-kind hysteresis* led Kovalev et al. [4,6] to interpret it as the *intra-layer boiling crisis* for the vapour layer formation inside the porous covering at the heating surface. They also proposed generalised boiling curves characteristic of a surface with a capillary-porous covering, Fig. 2, and regard *nucleation hysteresis*, curve 2, section A''–A as characteristic of porous structures of small pore diameters. This is also the reason why the superheating $\Delta T_{w,A''}$ is higher than for technically smooth surfaces. Point E marks the beginning of *nucleate boiling crisis*. If the vapour leaving the porous structure is hampered, the lowering of the heat flux takes place along the curves *EFG* or *DHB*. Curve *BFE* is realised in porous structures of low permeability. Hysteresis loops *EFG* and *DHB* result from the phenomenon of *capillary hysteresis*, which consists in the liquid flow from small diameter pores to larger ones being limited due to surface tension [6].

Capillary hysteresis results from pressure differences for adsorption (condensation) and desorption (evaporation), which take place on heating surfaces of changeable geometry and under the conditions of non-ideal wetting [2]. Hence, *intra-layer boiling crisis* or *capillary crisis* occurs when the

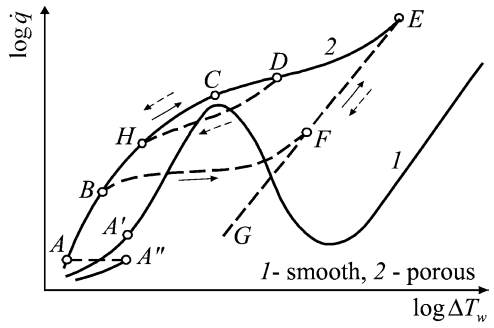

Fig. 2. Generalised boiling curves for capillary-porous surfaces [6].

forces of capillary suction are lower than the resistance of liquid and vapour flow through the porous layer [4,6].

2.4. II-kind hysteresis

II-kind hystereses, and boiling crisis hysteresis, Fig. 1(c) and (f), were first observed by Tehver et al., for Freon-113 on a flat aluminium surface with a bronze porous covering obtained with a plasma spraying technique [16]. They attribute changes in the boiling curve shapes, as those in Fig. 1(c) and (f), to changes in the amount of active pores. That results from inhomogeneity of pore diameter distribution in a porous covering. This concept was further developed by Poniewski et al. in their *II-kind hysteresis* model, based on vast experimental investigations into copper, fibrous, capillary-porous coverings [10,12,13]. *II-kind hysteresis* occurred in small thickness coverings ($\delta \leqslant 0.6$ mm) and with a liquid of the wetting angle smaller than that of water, i.e., Freon-113 and ethanol.

Fig. 3 presents a boiling curve, which generalises experimental results. A dotted line in this figure marks ranges of very small superheating ($\Delta T \sim 1$ K), not demonstrated in experimental boiling curves because of results distortion due to the measurement error. Their existence and shape, nevertheless, result from the development of heat transfer processes in a thin-layered porous structure.

Range "*k*", Fig. 3, covers the liquid convection and conduction in a porous layer.

Range "*o*" demonstrates pores activation on the structure external surface. In the structure of inhomogeneous pore dimensions distribution, there occurs a gradual activation of nucleation centres of smaller and smaller diameters D_a at the heating surface temperature increase up to ΔT_2, in accordance with Eq. (2), where $R = D_a/2$.

Because of the *II-kind hysteresis* formation mechanism, ranges "*a*", "*b*" and "*c*" are of particular importance.

Range "*a*". Nucleate boiling was clearly observed and the shape of the section "*a*" of the boiling curve ($\dot{q} \sim \Delta T_w^1$) points to unchangeable thermal resistance and a constant amount of active cells on the porous covering external surface, Fig. 4(a).

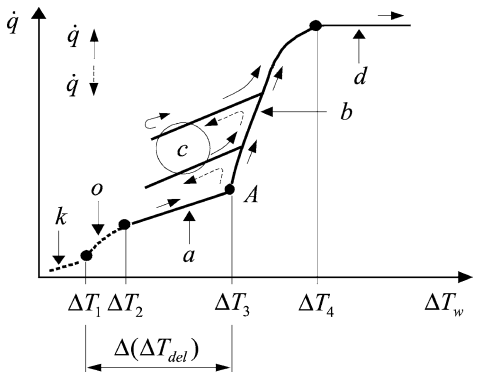

Fig. 3. Characteristic ranges of boiling curves for ethanol and Freon-113 and thin-layered porous structures [12,13].

Range "*b*". A dramatic change in the boiling curve inclination at point "*A*" means that the increase in heat flux is accompanied by a growing number of nucleation centres, $N = f(\dot{q})$. The activation of subsequent cells of smaller and smaller sizes takes place, Fig. 4(b).

Range "*c*". Hysteresis phenomenon, represented in Fig. 3 by curves "*c*", is revealed after the heat flux is diminished in range "*b*". The boiling curve shape indicates that pores activated in range "*b*" remain active despite reduced heat flux. That is the physical reason behind *II-kind hysteresis*.

While constructing the boiling model in ranges "*b*" and "*c*" with *II-kind hysteresis*, the authors relied on the work of Smirnov et al. [14]. In that model, an elementary cell of a capillary-porous covering was substituted with a fragment of finned surface as presented in Fig. 5. It was also assumed that it is the thermal resistance of liquid micro-layer covering vapour channels that decides about heat transfer. The model was extended to account for thin-layered structures by adopting an assumption of a finite height of a micro-fin and that of inhomogeneity of pore dimensions.

For very small superheating $\Delta T_w < \Delta T_1$, range "*k*", on the whole of the porous structure surface $A_1 = A$ ($f_1 = A_1/F = 1$), the heat flux amounts to

$$\dot{q}_1 = h_{cc}\Delta T_w \tag{10}$$

where h_{cc} stands for the equivalent heat transfer coefficient for conduction and convection. Beginning from $\Delta T_w = \Delta T_1$, there appears another heat transfer mechanism—boiling on the porous structure external surface, Fig. 3, range "*o*". With the increase in superheating, it affects larger and larger part A_2 of the total surface A. The fraction of

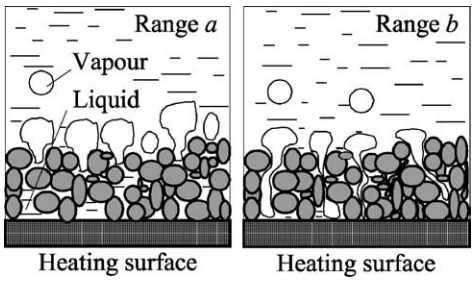

Fig. 4. Heat transfer mechanisms in ranges "*a*" and "*b*" [13].

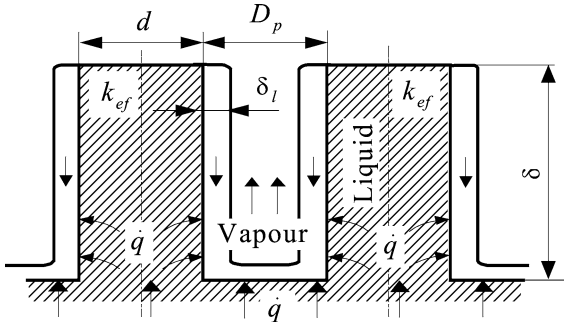

Fig. 5. Simplified model of an elementary cell of capillary-porous structure [14].

the structure external surface, on which boiling takes place, amounts to

$$f_2 = A_2/A = \int_{D_a}^{D_{p,max}} D_p^2 \gamma(D_p)\,dD_p \Big/ \int_{D_{p,min}}^{D_{p,max}} D_p^2 \gamma(D_p)\,dD_p \tag{11}$$

where the minimum diameter D_a of active pores depends on superheating ΔT_w^*, in accordance with Eq. (2). When the porous structure parameters are known, it is possible to determine characteristic superheatings ΔT_1 and ΔT_2, Fig. 3, by inserting into Eq. (2) the maximum and minimum pore diameter D_{max} and D_{min}, respectively.

Due to very small structure thickness and relatively high covering thermal conductivity, the structure conductivity thermal resistance is to be disregarded. In the area A_2, heat transfer process is expressed by

$$\dot{q}_2 = h_{sb}\Delta T_w \tag{12}$$

where h_{sb} is the experimentally determined boiling heat transfer coefficient for the structure external surface.

In the superheating range $\Delta T_1 < \Delta T_w < \Delta T_2$, section "*o*", Fig. 3, the total flux of transferred heat amounts to

$$\dot{q} = \underbrace{\dot{q}_1(1-f_2)}_{\substack{\text{conduction}\\ \text{and convection}}} + \underbrace{\dot{q}_2 f_2}_{\substack{\text{boiling on the}\\ \text{external surface}}} \tag{13}$$

In range "*a*", where $\Delta T_2 < \Delta T_w < \Delta T_3$ and $A_2 = A$ ($f_2 = A_2/A = 1$), the total heat flux is

$$\dot{q} = \dot{q}_2 \tag{14}$$

It is assumed that vapour phase formation takes place on the surface of liquid micro-layer, which covers vapour channel surface. A vapour channel, together with an adjacent skeleton, constitutes an elementary cell treated as a fragment of finned surface, Fig. 5.

On the basis of the condition that the sum of pressure drop in liquid and vapour jets moving in opposite directions should be smaller or equal to the capillary pressure increment, the boundary liquid micro-layer thickness δ_l was calculated [14]:

$$\Delta p_l + \Delta p_g \leqslant 4\sigma_{lg}/D_p \tag{15}$$

$$\delta_l \,\text{const}\big(\dot{q}^{cell}\nu_l D_p/h_{lg}\sigma_{lg}\big)^{0.4}(A_f/O)^{0.6}(k_{ef}/k_l)^{0.2} \tag{16}$$

where $\dot{q}^{cell}$ is the heat flux in a single porous structure cell, in which boiling takes place. The solution of the heat conduction equation for a micro-fin led to the determination of the heat flux $\dot{q}^{cell}$:

$$\dot{q}^{cell} = k_{ef} m(\Delta T_w - \Delta T^*) \times \left(\frac{h}{m\lambda_{ef}} + th(m\delta)\right) \Big/ \left(1 + \frac{h}{m\lambda_{ef}} th(m\delta)\right) \tag{17}$$

where ΔT^* is the temperature increment resulting from the action of capillary forces, determined from Eq. (2) for $D_a = D_p$. As $h = k_l/\delta_l$ and δ_l, in accordance with Eq. (16), depends on $\dot{q}^{cell}$, Eq. (17) is of implicit character and has to be solved numerically.

Similarly to what happened on the external side of the porous covering, range "*o*", gradual activation of cells of smaller and smaller diameter D_a^* also takes place inside the covering. When the boiling agent is the liquid of a small wetting angle, however, due to the phenomenon of potential nucleation centres flooding, the activation of pores inside is delayed in accordance with

$$D_a^* = 4\sigma_{lg}T_{sat}/\rho_g h_{lg}\big(\Delta T_w - \Delta(\Delta T_{del})\big) \tag{18}$$

where $\Delta(\Delta T_{del})$ is experimentally determined delay in pores activation inside the structure, Fig. 3.

Hence the fraction of the structure surface affected by internal boiling amounts to

$$f_3 = A_3/A = \int_{D_a^*}^{D_{p,max}} D_p^2 \gamma(D_p)\,dD_p \Big/ \int_{D_{p,min}}^{D_{p,max}} D_p^2 \gamma(D_p)\,dD_p \tag{19}$$

whereas the density of the heat flux transferred from active cells equals

$$\dot{q}_3 = (1-\varepsilon)\int_{D_a^*}^{D_{p,max}} \dot{q}^{cell}\gamma(D_p)\,dD_p \tag{20}$$

where term $1-\varepsilon$ is proportional to the area occupied by micro-fins.

One of the implications of the model assumed is that the total heat flux in range "*b*" of the boiling curve can be calculated from

$$\dot{q} = \underbrace{\dot{q}_2(1-f_3)}_{\substack{\text{boiling on the}\\ \text{external surface}}} + \underbrace{\dot{q}_3 f_3}_{\substack{\text{boiling inside}\\ \text{the covering}}} \tag{21}$$

To sum up the reasoning presented so far, the process of heat transfer on thin-layered porous surface in ranges "*k*", "*o*", "*a*" and "*b*" of the boiling curve can be expressed with a single equation

$$\dot{q} = \big(\dot{q}_1(1-f_2) + \dot{q}_2 f_2\big)(1-f_3) + \dot{q}_3 f_3 \tag{22}$$

where the quantities $\dot{q}_1$, $\dot{q}_2$ and $\dot{q}_3$ as well as A_2 and A_3 are described with formulas (10)–(12), (19), (20), respectively. Fig. 6 presents, in a symbolic way, the sequence and co-occurrence of individual mechanisms in heat transfer process together with the areas they affect for subsequent boiling curve ranges.

If there occurs a decrease in heat flux, range "*c*", before superheating ΔT_4 is reached, Fig. 3, the cells participating in boiling process will remain active although their diameters may become smaller than D_a^*. In other words, if the heat flux decrease takes place at superheating ΔT_{hst}, the area affected by boiling inside the structure remains unchanged

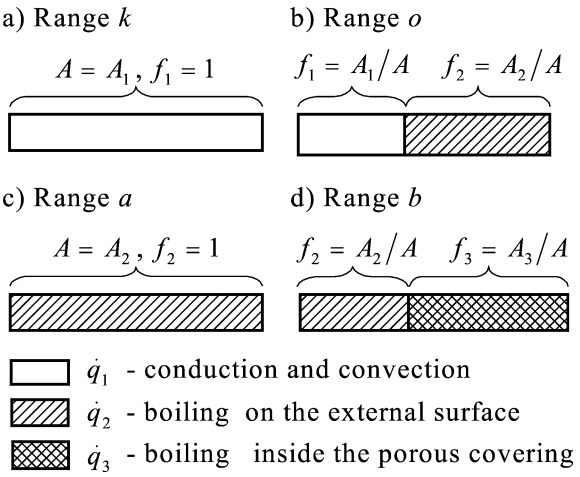

Fig. 6. Occurrence and reach of heat transfer mechanisms for subsequent ranges of boiling curve [13].

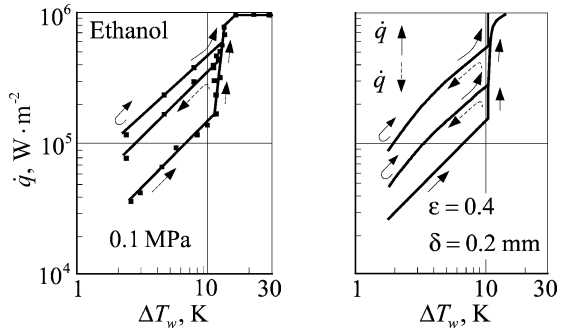

Fig. 7. Experimental and theoretical boiling curves with *II-kind hysteresis* [10,12,13].

and equals A_{hst}. The constant fraction of the active area $f_{\mathrm{hst}} = A_{\mathrm{hst}}/A$ can be calculated by inserting $D_{\mathrm{a}}^{*} = D_{\mathrm{hst}}^{*}$ into Eq. (19). Thus the heat flux density dependence on superheating in range "*c*" of the boiling curve can be calculated on the basis of

$$\dot{q} = \dot{q}_2(1 - f_{\mathrm{hst}}) + \dot{q}_3 f_{\mathrm{hst}} \tag{23}$$

The above equation, together with Eq. (22), provides a mathematical description of a boiling curve with *II-kind hysteresis*.

The comparison of calculation results and experimental data was presented in Fig. 7. The results of theoretical calculations are qualitatively, and to some extent quantitatively, congruent with the experimental data [12,13].

3. Boiling crisis

Boiling crisis in porous layers cannot be understood in the same way as for a smooth surface. Experimental investigations show that the heating surface temperature increase is not so vehement and the heat transfer coefficient diminishes in a gentle manner. Thus the *critical heat flux* $\dot{q}_{\mathrm{c}}$ for developed micro-surfaces and capillary porous structures is often termed the *maximum heat flux* $\dot{q}_{\max}$.

There are plenty of factors which affect boiling crisis: the type of industrial micro-surface or capillary porous structure, the structure thickness, the size of pores and the distribution of their diameters, the boiling liquid thermal properties and the way the porous layer is supplied with the liquid. They all contribute to the phenomenon complexity. Investigators, therefore, comment on *the decrease in the heat transfer coefficient* value, *the structure being filled with vapour*, *intra-layer crisis* or *capillary crisis* preceding *nucleate boiling crisis* or *heat flux corresponding to the maximum heat transfer coefficient*.

By analogy with technically smooth surfaces, *nucleate boiling crisis* is most frequently thought to begin together with the formation of a stable, continuous, thin vapour layer outside the external surface of the capillary structure. A different character of nucleate boiling on industrial developed micro-surfaces and capillary-porous coverings, as well as the multitude of factors affecting the phenomenon, account for serious difficulties in its modelling.

Experimental data concerning mesh structures and those of sintered powders led to the construction of *two hydrodynamic models of nucleate boiling crisis*.

The model of Smirnov et al. [1,15], related to mesh porous structures, assumes that the crisis occurs when the stability of wall adjacent two-phase layer is lost. This happens when the kinetic energy of the vapour generated inside the capillary porous structure is greater than, or equal to the energy of the potential two-phase layer at the heating surface:

$$\left(\dot{q}_{\mathrm{c}}/h_{\mathrm{lg}}\rho_{\mathrm{g}}\right)^2 \rho_{\mathrm{g}} \geqslant k_1^2\,(\rho_{\mathrm{l}} - \rho_{\mathrm{g}})\left(\sigma_{\mathrm{lg}} g/(\rho_{\mathrm{l}} - \rho_{\mathrm{g}})\right)^{1/2} \tag{24}$$

where $\dot{q}_{\mathrm{c}}$ is the critical boiling heat flux for a smooth surface consistent with hydrodynamic Kutateladze–Zuber hypothesis. In order to emphasise the difference in the phenomenon character on capillary-porous coverings, the characteristic heat flux was marked $\dot{q}_{\max}$.

The work of friction forces during vapour transportation through the capillary porous covering gives the following energy balance:

$$E_{\mathrm{k}}''' \geqslant k_1^2 E_{\mathrm{2ph}}''' - k_2 E_{\mathrm{f}}''' \tag{25}$$

where E_{k}''' is the kinetic energy of the vapour jet, E_{2ph}'''— the potential energy of the two-phase layer near the heating surface, being the right part of Eq. (24), E_{f}''' is the work of friction forces for the vapour passing through the covering. *The maximum heat flux* $\dot{q}_{\max}$ can be evaluated in the same way as in Eqs. (24) and (25):

$$E_{\mathrm{k}}''' = \left(\dot{q}_{\max}/h_{\mathrm{lg}}\rho_{\mathrm{g}}\right)^2 \rho_{\mathrm{g}} \tag{26}$$

The potential energy of a stable two-phase layer can be calculated from

$$k_1^2 E_{\mathrm{2ph}}''' = C_1\left(\dot{q}_{\mathrm{c}}/h_{\mathrm{lg}}\rho_{\mathrm{g}}\right)^2 \rho_{\mathrm{g}} \tag{27}$$

While formulating expression (24), the existence of only one source of potential energy was assumed, E'''_{2ph}. Therefore, the presence of the porous covering should lead to the decrease in $\dot{q}_{max}$, which disagrees with experimental data. During a boiling process, the curvilinear interface is formed by capillary forces inside the covering cells closest to the heating surface. This factor can be regarded as a new source of potential energy, which could be calculated from Laplace equation

$$k_3 E'''_\sigma \approx C_3 4\sigma_{lg}/D_p \tag{28}$$

where E'''_σ is the potential energy developed by capillary forces.

In boiling, an intensive entrainment of liquid droplets outside the porous layer takes place, causing an additional loss of kinetic energy, $\Delta E'''_{ej}$. The modified energy stability condition for two-phase layer, which provides for all considerations above, Fig. 8, will be as follows:

$$E'''_k \geqslant k_1^2 E'''_{2ph} - k_2 E'''_f + k_3 E'''_\sigma - \Delta E'''_{ej} \tag{29}$$

Another extreme condition, occurring mainly in heat pipes, is usually called *hydrodynamic limit*. For $\dot{q}_{max}$, this limit is calculated from the condition of inequality of capillary pressure and hydraulic resistance of the liquid flow inside the porous layer reduced or augmented by hydrostatic pressure:

$$4\sigma_{lg}/D_p \leqslant \mu_l u_l L/K \pm \rho_l g H \tag{30}$$

where u_l is the liquid velocity inside the porous layer, K is the structure permeability and L is the maximum liquid transportation path, Fig. 8. The mass flux of the liquid is equal to the mass flux of the vapour generated inside the porous covering. On the basis of this balance, the velocity u_l is calculated

$$u_l = q_{max} A/h_{lg}\rho_l n\delta O \tag{31}$$

where O is the perimeter of the heating surface, δ is the thickness of a single screen layer and n is the number of the layers. The complete energy condition for *the boiling crisis* should be a combination of both conditions (29) and (30). A discussion of detailed forms of individual terms in Eqs. (29) and (30) was presented in [1,15]. After the introduction of necessary simplifications, the final result of the considerations presented above can be given in the form

$$Z = C_4\left(\sqrt{1 + C_5 Y} - 1\right) \tag{32}$$

where

$$Z = \dot{q}_{max}\left(f(\varepsilon)/h_{lg}\rho_g\nu_l A\right)(K^* On\delta/L)$$
$$Y = \left\{f(\varepsilon)\left((4\sigma_{lg}/D_p) \pm \rho_l g H\right)/\rho_g A^2 \nu_l^2\right\}(K^* On\delta/L)^2 \tag{33}$$

The experimental data were obtained for a flat circular copper heating surface, covered with various screen metallic layers. The number of screen layers n changed from 1 to 24, the cell size ranged 0.04–0.5 mm, the saturation pressure was 0.01–0.1 MPa [1,15]. Eq. (32) matches the experimental data concerning the screen porous covering for water and ethanol when $C_4 = 1.8 \times 10^{-5}$ and $C_5 = 2.21 \times 10^5$. The approximating curve in Fig. 9 is the best visual fit of the experimental data with the scatter reaching, in extreme cases, ±50%.

The hydrodynamic model by Kovalev et al. [5,7] substituted a real capillary porous structure with a system of vertical cylindrical capillaries connected with one another by means of horizontal channels, Fig. 10. For the heat flux values close to the critical one, $\dot{q} \leqslant \dot{q}_c$, a vapour layer is formed

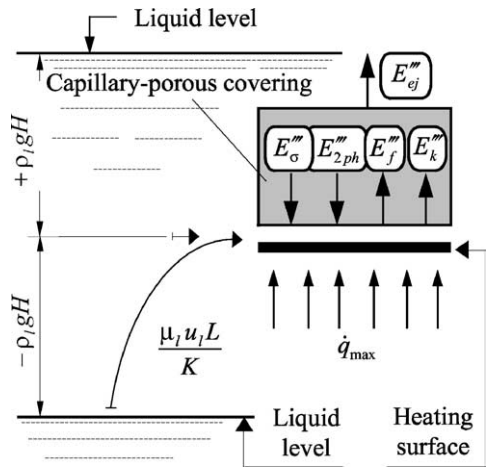

Fig. 8. Graphic illustration of energy stability condition for two-phase layer inside capillary-porous covering, Eq. (29), and the hydrodynamic limit, Eq. (30) [1].

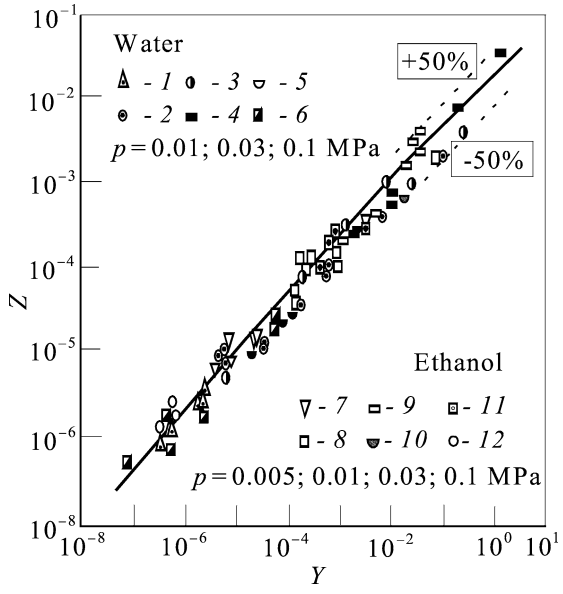

Fig. 9. Generalisation of the experimental data for screen porous coverings: 1—stainless steel (SS), $D_p = 0.04$ mm, $n = 2, 3$; 2—SS, $D_p = 0.06$ mm, $n = 2, 3, 4, 5, 10, 24$; 3—SS, $D_p = 0.125$ mm, $n = 2, 3, 4, 5, 9$; 4—SS, $D_p = 0.2$ mm, $n = 2, 3, 4, 5, 9$; 5—brass, $D_p = 0.08$ mm, $n = 2, 3, 5$; 6—copper, $D_p = 0.045$ mm, $n = 2, 3, 5$; 7—SS, $D_p = 0.06$ mm, $n = 2, 9$; 8—SS, $D_p = 0.125$ mm, $n = 2, 3, 8$; 9—SS, $D_p = 0.45$ mm, $n = 2, 3$; 10—brass, $D_p = 0.08$ mm, $n = 3, 9$; 11—brass, $D_p = 0.16$ mm, $n = 2, 3$; 12—copper, $D_p = 0.045$ mm, $n = 2$; [1,15].

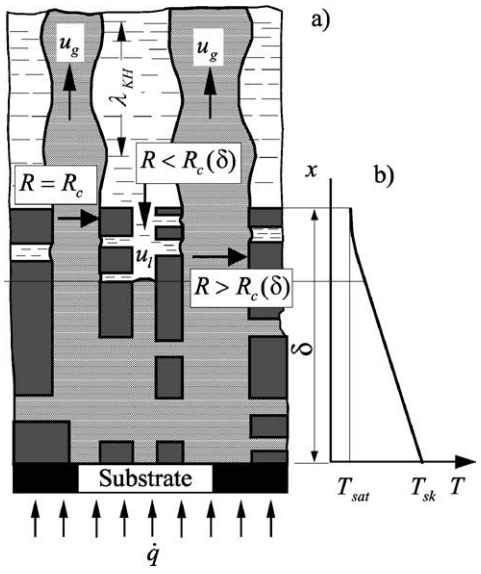

Fig. 10. Heat transfer model for $\dot{q} \leqslant \dot{q}_c$: (a) evaporation front location inside the capillary-porous structure, (b) temperature distribution [7].

inside the porous covering, which is adjacent to the heating surface. The heat flux is transferred through the vapour layer to the boiling front inside the covering. Hence the heating surface superheating is much higher than for a smooth surface.

The maximum vapour velocity in a capillary, Fig. 10, was determined on the basis of stream stability condition in accordance with Kelvin–Helmholtz's stability hypothesis:

$$u_{g,\max} = \left\{2\sigma_{lg}\rho_l \big/ \left(\Pi(R_p)\rho_g(\rho_l+\rho_g)R_p\right)\right\}^{1/2} \tag{34}$$

According to this hypothesis, vapour jets are stable for much higher vapour velocities than in Taylor's model and it gives $\dot{q}_{\max} \geqslant \dot{q}_c$. Prior to determining the participation of pores acting as vapour channels, it is necessary to calculate the radius of liquid meniscus on the external surface of the porous covering from

$$2\sigma_{lg}/R_c(\delta) = \Delta p_{pf} + \rho_g(u_g)^2 \tag{35}$$

It describes the balance of liquid and vapour phases at the outlet of a porous covering. Pores of the radius $R_p > R_c(\delta)$ are filled with vapour and pores with $R_p < R_c$ with liquid, Fig. 10. The vapour maximum velocity at the porous covering outlet corresponds to the radius of the liquid volume perforation through the vapour jet, $R = R_{pf}$, which is determined from Eqs. (34) and (35):

$$R_c(\delta) = \pi R_{pf}\rho_l \big/ \left((\pi+1)\rho_l + \rho_g\right) \tag{36}$$

where for $\rho_g \ll \rho_l$, $R_c(\delta) \cong 0.76R_{pf}$.

The maximum density of the heat flux is obtained by summing up vapour jets with reference to the porous covering surface unit:

$$\dot{q}_{\max} = \varepsilon h_{lg}\rho_g \int_{R_c}^{R_{\max}} u_g(R_p)\gamma(R_p)\,\mathrm{d}R_p$$

$$= \varepsilon h_{lg}\sqrt{\frac{2\sigma_{cg}\rho_g\rho_l}{\pi(\rho_g+\rho_l)R_{pf}}}\left(1-\Pi\left(R_c(\delta)\right)\right) \tag{37}$$

The approximate value of $\Pi(R_c(\delta))$ was determined from the percolation theory, as well as on the basis of the data obtained from a numerical experiment for structures sintered from spherical particles [2]. For the most frequently applied coverings of sintered powders the following can be stated:

$$\dot{q}_{\max} = 0.52h_{lg}\varepsilon^{2.28}\left(\sigma_{lg}\rho_l\rho_g/(\rho_l+\rho_g)R_{pf}\right)^{1/2} \tag{38}$$

The theoretical values $\dot{q}_{\max}$ calculated on the basis of Eq. (38) range from 0.52 to 1.44 of the experimental values for water, ethanol, Freon-113 and nitrogen for boiling on coverings of copper and bronze sintered powders [7].

Poniewski et al. [11] put forward *a model of intra-layer boiling crisis* based on *the concept of the maximum point process*. It was assumed that the distribution of pores in the covering could be always described with two-dimensional Poisson point process of constant intensity, proportional to the number of pores per surface unit. It was also assumed that the rule, which decides about a porous cell being filled with vapour as the surface superheating function, is expressed in the form of a thinning function $p = p(x)$. Under given heat transfer conditions, it ascribes a certain probability $p(x)$ to each cell x.

In other words, the distribution of dried sites of the porous covering can be modelled mathematically with the so-called thinned point process N_p, the one originating from process N through randomly "cutting out" its location in accordance with probability $p(x)$. It is worth mentioning that the process formed in this way is also Poisson process of certain intensity λ.

The process of the porous covering drying up as the function of increasing superheating ΔT_w is, if this approach is adopted, a statistical process. There exists a certain critical level of drying intensity ν, the exceeding of which in a random area of the heating surface causes the covering drying up. Level $\nu(A)$ is a measure proportional to the field of the dried surface A. At the same time the proportionality constant b provides information about the lowest number of cells per surface unit which must be dried up for vapour film to be formed inside the covering. It means that the occurrence of *intra-layer heat transfer crisis* is equivalent to *the maximum point process* exceeding the critical intensity level in a random area of the covering, larger than the critical one, A_c.

Values of parameters a, b, A_c, $p_1, \ldots, p_n$ (see nomenclature) were assumed. They depend on the structure geometrical properties and thermal properties of both the structure and the liquid. The probability p^* of *intra-layer boiling crisis* non-occurrence was estimated for the series of superheatings $T_1, \ldots, T_n$:

$$\mathrm{e}^{-(f+1)\lambda}\left(\sum_{k=0}^{\nu}\frac{\lambda^k}{k!}\right)^{f+1} \leqslant p^* \leqslant \mathrm{e}^{-f\lambda}\left(\sum_{k=0}^{\nu}\frac{\lambda^k}{k!}\right)^{f} \tag{39}$$

where

$$p = 1 - p^*, \qquad \nu = [bA_c],$$
$$\lambda = aA_c\{1 - (1 - p_1)\ldots(1 - p_n)\}, \qquad f = [F/A_c] \quad (40)$$

and the symbol $[x]$ denotes the integer part of the number x.

Hence the probability of crisis occurrence is, in particular, the function of the heating surface superheating range ΔT_w, for a given covering and liquid, it is, therefore, possible to find the value of permissible superheating, which will be smaller than the pre-set safety level. It is also possible to calculate the superheating value, for which *intra-layer boiling crisis* occurs. Such methodology allows numerical simulation of *nucleate boiling crisis* formation in porous structures.

The model (39) underwent initial verification for a metal fibrous covering, Fig. 11. With $\dot{q}$ approaching 1.7×10^5 W·m^{-2} (this is the experimental value of $\dot{q}_{max}$), the probability approaches 1, which means that the model (39) describes the phenomenon under investigation in a satisfactory manner. The impact of the magnitude of the critical field c on *intra-layer boiling crisis* occurrence was also investigated. The dependence obtained proved to be monotone, decreasing, Fig. 11(b), and congruent with the intuitive understanding of the phenomenon being considered.

An interesting and sophisticated approach, both theoretical and experimental, to the critical (maximum) heat flux enhancement was proposed by Liter and Kaviany [8]. They applied modulated porous coatings with periodically non-uniform, designed variations in the covering thickness, Fig. 12. The coverings were made from sintered spherical copper particles by dry-phase diffusion in a reducing atmosphere. The imposed modulation was assumed to create alternating regions of low resistance to vapour escape and highly capillary-assisted liquid draw. This should facilitate liquid-vapour counter flow within the capillary-porous layer and enhance boiling heat transfer from the substrate to the liquid pool in a manner similar to heat pipes.

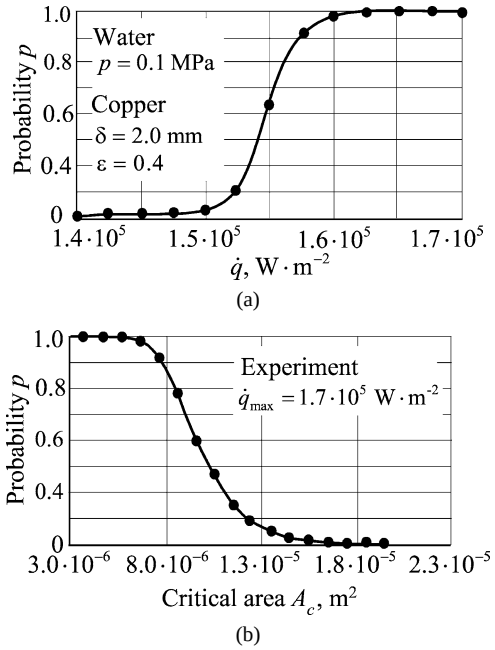

Fig. 11. The dependence of *intra-layer boiling crisis* occurrence probability $p = 1 - p^*$ on values of: (a) heat flux; (b) assumed critical area [11].

For the investigated porous covering design, various possible physical limitations causing *nucleate boiling crisis* were considered. The limitations ranged from counter flow limit for a deep porous layer (the lowest $\dot{q}_{max}$) to kinetic evaporation limit (the highest $\dot{q}_{max}$). Some simplifying assumptions were made, as regards the flow paths, without rigorous experimental validation in order to develop models that would allow to calculate the boiling curve $\dot{q} = \dot{q}(\Delta T_w)$ and the $\dot{q}_{max}$. The most important assumptions were as follows:

(a) separated liquid and vapour mass fluxes within the covering space, Fig. 12;
(b) local thermal equilibrium in all phases;
(c) Darcy–Ergun momentum equation with Leveret J-function relating the liquid saturation, porosity, permeability and wettability to capillary pressure;
(d) energy equation for volume-averaged values of the liquid local temperature and the stagnant thermal conductivity of the porous covering;
(e) viscous–drag numerical model, which defines the evaporation rate at the liquid–vapour interface and the heat flux at the bottom of the porous covering;
(f) hydrodynamic liquid–choking limit, $\dot{q}_{max} = \dot{q}_{max,h}$, which determines the ability of the liquid to flow towards the heating surface through the escaping vapour; the limit determines the highest heat flux $\dot{q}_{max}$, at which the liquid is able to reach the heating surface.

Numerical solution of the momentum and energy equations for the viscous drag numerical model and the wetted surface regime, Fig. 12, allowed the prediction of the slope of $\dot{q}_{vs}$ versus ΔT_w curve. The model underestimates the $\dot{q}_{vs}$ as the function of ΔT_w, but it can be considered to be in fair agreement with the experimental dashed line, Fig. 13, despite many assumptions that were made. The authors [8]

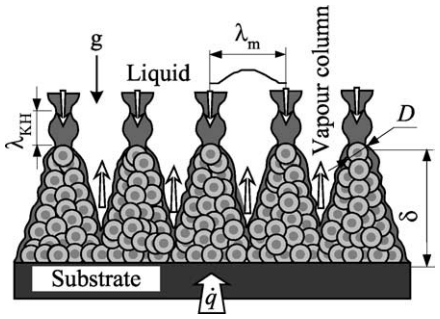

Fig. 12. Scheme of the physical model of liquid–vapour interface hydrodynamic instability limit for the liquid reaching the surface at boiling on modulated porous covering [8].

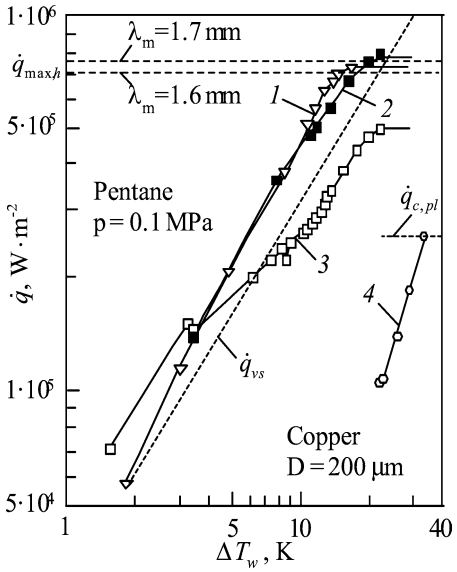

Fig. 13. Experimental data for various porous coverings: 1 – single modulated, $\delta = 6D$, $\lambda_m = 5D$; 2 – double modulated, $\delta = 5D$ and $9D$, $\lambda_m = 8D$; 3 – uniform layer, $\delta = 3D$; 4 – plain surface [8].

conclude that the assumptions regarding liquid flow paths and volume averaging of the porous media should be reconsidered to make the result of numerical calculations show higher congruence with the experiment. It was also assumed that modulation of the porous covering imposes a geometrically determined, i.e., modulated, critical wave length λ_m, Fig. 12, which supersedes the dependence on the Rayleigh–Taylor wave length and extends the hydrodynamic choking limit. This way of thinking led to a very simple final expression for $\dot{q}_{max}$:

$$\dot{q}_{max,h} = (\pi/8)h_{lg}(\sigma_{lg}\rho_g/\lambda_m)^{1/2} \tag{41}$$

For the porous coverings tested by Liter and Kaviany [8], the $\dot{q}_{max}$ is shown to be hydrodynamically limited, $\dot{q}_{max} = \dot{q}_{max,h}$, Fig. 13. The congruence of the theory and the $\dot{q}_{max,h}$ experimental data, Fig. 13, is presented in a slightly obscure manner. For the dual-height modulation covering, the experimental $\dot{q}_{max}$ corresponds to $\dot{q}_{max,h}$ for $\lambda_m = 1.46$ mm predicted from Eq. (41) and the real $\lambda_m = 1.6$ mm. For single-height modulation, the appropriate values of λ_m are 1.68 and 1 mm, respectively; the difference is quite substantial.

One of the obvious advantages of the presented hydrodynamic model is high congruence of measured and calculated values of $\dot{q}_{c,pl}$ for a flat porous covering, Fig. 13. The investigated modulated capillary-porous coverings provide a noticeable increase in $\dot{q}_{max}$ and a decrease in ΔT_w when compared with a flat coverings tested in this study, Fig. 13, and reported in the literature [1,5,9,11]. The authors [8] predict that further enhancement of the $\dot{q}_{max}$ in the modulated capillary-porous covering can be done by the reduction of the modulated wave length λ_m and the particle size D, and by removing the limiting hydrodynamic mechanism.

4. Conclusions

Nucleation hysteresis, Fig. 1(a), is far more strongly manifested on capillary-porous coverings than on technically smooth and flat surfaces. The phenomenon is affected by the following factors: wetting angle θ and its dynamic variation in the liquid motion function, penetration properties of the boiling liquid and various geometry of vapour filled pores in the processes of boiling incipience and fading [3,9,16]. An additional factor enhancing *nucleation hysteresis* in porous structures can be thermo-capillary convection in the liquid micro-layer covering the walls of the structure skeleton [9].

I-kind hysteresis (*hysteresis with memory*, *intra-layer boiling crisis*), Fig. 1(b), occurs when the forces of capillary drag are smaller than the liquid and vapour resistance in the flow through the capillary-porous layer [9]. That means condition (15) is not satisfied and vapour layer persists inside the porous covering.

II-kind hysteresis, Fig. 1(c), results from two subsequent phenomena. The first one is the flooding of potential nucleation centres with boiling liquid, which takes place for small values of surface superheating ΔT_w. When the nucleation process is fully developed and the superheating ΔT_w has reached an appropriately high value, pores activated while heat flux was increasing, still remain active after heat flux has decreased. It is the thermal resistance of the liquid micro-layer covering vapour channels that decides about heat transfer [12,13].

In their modelling of the *nucleate boiling crisis*, most authors rely on well-established hypotheses that liquid–vapour interface demonstrates hydrodynamic stability, Smirnov et al. [1,15], Kovalev et al. [5,7] and Liter and Kaviany [8]. Only Poniewski et al. [11] suggest that boiling crisis might be treated as the maximum point process, which develops inside the porous layer. Both hydrodynamic models and that based on the maximum point process approach indicate that the maximum heat flux density for capillary-porous coverings depends, in a complex manner, on the porous layer structural parameters, boiling liquid thermal and penetration properties and their mutual relation. For hydrodynamic approach it is necessary to assume a simplified geometry of porous structure and, consequently, a simplified model of vapour and liquid flows inside the structure. Liter and Kaviany say, quite rightly, that assumptions of that kind are made without rigorous experimental validation [8].

All the models of hysteresis and nucleate boiling crisis discussed in the paper made assumptions about the physics of heat transfer at the level of a single cell of a porous structure. The results obtained for those models were verified, however, on the basis of experimental investigations into a large set of porous cells, i.e., the whole porous covering of the heating surface. That means none of the models of hysteresis phenomena or boiling crisis discussed in the paper was confirmed by experimental investigations, either in a single pore cell or in a set of neighbouring cells. All models discussed rely on hypothetically assumed mechanism of

heat transfer. As they were worked out and experimentally verified for a single type of a porous covering, their usefulness for practical applications is not particularly high.

The knowledge of the boiling crisis and heat transfer hysteresis phenomena broadens mainly owing to experimental investigations. As researchers cannot agree about the mechanisms of heat transfer and often obtain contradictory experimental results, it is necessary to conduct elementary research. The following issues should be examined in particular:

(a) visualisation of the liquid micro-layer covering the skeleton of the porous structure (it would allow to measure the liquid layer thickness and velocities of the liquid and the vapour inside the structure);
(b) nucleation in porous layers (nucleation at superheatings lower than those on smooth surfaces and delayed boiling incipience);
(c) conditions of intra-layer boiling crisis occurrence;
(d) impact of the materials a porous covering is made of and its geometry and also physical properties of heat agent on the boiling curve shape.

Only such detailed and sophisticated experimental investigations can help verify discussed hypotheses and broaden the knowledge of nucleate boiling inside a capillary-porous layer.

References

[1] B.A. Afanas'ev, G.F. Smirnov, M.E. Poniewski, Boiling crisis heat flux in capillary porous layer, Arch. Thermodynam. 16 (3–4) (1995) 165–175.
[2] L.I. Chejfec, A.V. Nejmark, Multiphase Processes in Porous Media, Chimija, Moscow, 1982 (in Russian).
[3] S. Ko, B. Liu, Y. Yao, Boiling hysteresis on porous metallic coatings, in: Proc. II Int. Symp. Multiphase Flow and Heat Transfer, vol. 1, Beijing, 1989, pp. 258–268.
[4] S.A. Kovalev, V.A. Len'kov, Mechanism of burnout with boiling on a porous surface, Thermal Engrg. 28 (4) (1990) 201–203.
[5] S.A. Kovalev, S.L. Solov'ev, Heat transfer and critical heat fluxes in boiling on a porous surface, Heat Transfer–Soviet Res. 22 (3) (1990) 364–375.
[6] S.A. Kovalev, S.L. Solov'ev, O.A. Ovodkov, Liquid boiling on porous surfaces, Heat Transfer–Soviet Res. 19 (1) (1987) 109–120.
[7] S.A. Kovalev, S.L. Solov'ev, O.A. Ovodkov, Theory of boiling heat transfer on a capillary-porous surface, in: Proc. X Int. Heat Transfer Conf., vol. 2, Jerusalem, 1990, pp. 105–110 (paper 1-BO-18).
[8] S.G. Liter, M. Kaviany, Pool boiling CHF enhancement by modulated porous-layer coating: theory and experiment, Internat. J. Heat Mass Transfer 44 (2001) 4287–4311.
[9] S.P. Malyshenko, M.A. Styrikovich, Heat transfer at pool boiling on surfaces with porous coating, in: Proc. II Int. Symp. Multiphase Flow and Heat Transfer, Beijing, 1989, pp. 269–284.
[10] M.E. Poniewski, T.M. Wojcik, Experimental investigation of boiling heat transfer hysteresis on metal fibrous porous coverings, Arch. Thermodynam. 20 (1999) 93–118.
[11] M.E. Poniewski, M.L. Wisniewski, T.M. Wojcik, Heat transfer crisis on porous surfaces—Experimental investigations and outline of the maximum point process raised model, in: Scientific Papers of Kielce University of Technology, s. Mechanics, vol. 7, 1999, pp. 323–338.
[12] M.E. Poniewski, M.L. Wisniewski, T.M. Wojcik, Boiling heat transfer on metal fibrous porous surfaces—Experiment, model and verification, in: Phenomena and Emerging Applications, vol. 1, Boiling'2000, Begel House, 2000, pp. 772–788.
[13] M.E. Poniewski, M.L. Wisniewski, T.M. Wojcik, Probabilistic model of boiling heat transfer in thin-layer porous structures, Arch. Thermodynam. 21 (2000) 55–73.
[14] G.F. Smirnov, A.L. Coba, B.A. Afanas'ev, The heat transfer by boiling in splits, capillaries, wick structures, 1978, AIAA paper 78-461, p. 8.
[15] G.F. Smirnov, B.A. Afanas'ev, Investigation of vaporization in screen wick-capillary structures, in: Proc. IV Heat Pipe Conf., London, 1982, pp. 405–413.
[16] H. Zhang, Y. Zhang, Hysteresis characteristic of boiling heat transfer from powder-porous surface, in: Advances in Phase Change Heat Transfer, Academic Press, China, 1988, pp. 98–103.